uc3m | Universidad Carlos III de Madrid

e-Archivo

This is an accepted version of the following published document:

Vadillo, G.; Reboul, J.; Fernández-Sáez, J. (2016). A modified Gurson model to account for the influence of the Lode parameter at high triaxialities. *European Journal of Mechanics. A/Solids*, vol. 56, pp. 31-44.

DOI: https://doi.org/10.1016/j.euromechsol.2015.09.010

Copyright © 2015 Elsevier Masson SAS. All rights reserved.

This work is licensed under a
Creative Commons Attribution-NonCommercial-NoDerivatives 4.0 International License

A modified Gurson model to account for the influence of the Lode parameter at high triaxialities

G. Vadillo*, J. Reboul, J. Fernández-Sáez

Department of Continuum Mechanics and Structural Analysis. University Carlos III of Madrid. Avda. de la Universidad, 30. 28911 Leganés, Madrid, Spain

Abstract

The influence of the Lode parameter on ductile failure has been pointed out by different authors even at high triaxiality stress states. However, one of the most widely used model for ductile damage, like the Gurson-Tvergaard (GT) model, systematically disregard the role played by the third stress invariant. In this paper, an improvement of the classical Gurson-Tvergaard model is proposed. The new relation takes into account the effect of triaxiality and Lode parameter through the q_1 and q_2 GT parameters. The convexity of the proposed yield surface has been examined and ensured. The integration of the new constitutive equations as well as the consistent tangent modulus have been formulated and implemented in a Finite Element code. A computational $3D$ cell has been used to prescribe both macroscopic triaxiality and Lode parameter during loading. Numerical simulations are presented for Weldox 960 steel with different initial porosities and for different prescribed macroscopic triaxialities and Lode parameters using a computational $3D$ cell methodology. The results are compared with those obtained with a J_2 voided cell. These comparisons show that the improved model captures adequately the Lode effect on the stress-strain curves and on the void growth.

Keywords: Gurson model, Lode parameter, Consistent integration, Cell model analysis

1. Introduction

The ductile fracture phenomenon in metals and alloys usually follows a failure mechanism involving nucleation, growth and coalescence of voids. Pioneering micromechanical

*Corresponding author. Tel. +34916248460; Fax: +34 916249430. E-mail address: gvadillo@ing.uc3m.es

studies of this phenomenon were carried out by McClintock (1968); Rice and Tracey (1969) considering the growth of isolated cylindrical or spherical voids driven by plastic deformation of the surrounding rigid perfectly plastic matrix material. To analyze the ductile failure of porous materials, the Gurson-Tvergaard's damage model (Gurson, 1977; Tvergaard, 1981, 1982) is the most widely used approach. Tvergaard (1981, 1982) modified the Gurson model by introducing the q_1 and q_2 parameters to more accurately describe the void growth kinetics observed in unit cell computations. Faleskog et al. (1998) and Gao et al. (1998) have shown that these values are not constant but depend on both strength and strain-hardening properties. More recently, Kim et al. (2004) and Vadillo and Fernández-Sáez (2009) have pointed out that the q_i parameters also depend on the triaxiality of the stress field, as well as on the initial porosity, and highlighted the importance of a proper choice of q_1 and q_2 for the correct modelling of the void growth process.

Various extensions of the Gurson model have been developed and provided elsewere in order to better represent the response of ductile metals (Gologanu et al., 1997; Gărăjeu et al., 2000; Pardoen and Hutchinson, 2000; Zhang et al., 2000; Benzerga, 2002; Flandi and Leblond, 2005 b; Monchiet et al., 2008). These modifications make all the assumption of axisymmetric cavities remaining spheroidal during plastic deformation. For a review on constitutive models developed to simulate ductile failure up to recent times, see Besson (2010); Pineau and Pardoen (2007).

In the last years, several researchers (Zhang et al., 2001; Kim et al., 2003, 2004; Bao and Wierzbicki, 2004; Wen et al., 2005; Gao and Kim, 2006; Kim et al., 2007; Xue, 2007; Barsoum and Faleskog, 2007; Xue, 2008; Bai and Wierzbicki, 2008; Brünig et al., 2008; Gao et al., 2009, 2011; Barsoum and Faleskog, 2011; Barsoum et al., 2011; Jackiewicz, 2011; Danas and Ponte-Castañeda, 2012; Benallal et al., 2014) outlined that the stress triaxiality measure by itself is insufficient to caracterize plastic yielding, and highlighted the role of the third invariant of the deviatoric stress tensor, on void growth rates and other aspects of void behaviour which play an important role in strain softening and localization.

At high triaxialities, where the controlling damage mechanism is the void growth, the influence of Lode parameter can be also important (Barsoum et al., 2011). This effect cannot be properly accounted for with the classical GT model. At low triaxialities, the

source of the instability cannot be identified with a void growth mechanism (Yamamoto, 1978). The GT model was recently modified to introduce a Lode dependent softening term for low triaxialities (Nahshon and Hutchinson, 2008). By construction, this modification is inconsistent with mass conservation (Danas and Ponte-Castañeda, 2012).

In the present paper, an improvement of the Gurson-Tvergaard model that accounts for the influence of the Lode parameter at high triaxiality stress states is presented. The modification consists on incorporating the Lode parameter effect into the GT yield surface through q_1 and q_2, which depend not only of the stress triaxiality T, but also on the third invariant of the deviatoric stress tensor J_3. This new term is calibrated to ensure the convexity of the yield surface. The integration of the new constitutive equations has been implemented using a full implicit Euler-backward scheme combined with the return mapping algorithm. Additionaly, the consistent tangent modulus has been formulated. For validation purposes, a 3D extension of the computational cell model employed by Xia and Shih (1995 a,b, 1996) has been developed extending the prescription to both macroscopic triaxiality and Lode parameter. Numerical simulations using the Finite Element code ABAQUS/Standard (Simulia, 2014) are presented for Weldox 960 steel considering different initial porosities and various prescribed macroscopic triaxialities and Lode values. The obtained results using the new continuum damage model are compared with those found with a J_2 voided cell for both the void growth and the stress-strain response of the material.

2. Unit-3D cell model with prescribed triaxiality and Lode parameter

2.1. The unit-cell model

Under the assumption of a periodic microstructure, a porous material can be approximated by representative volume elements (RVE), each containing a void. The axisymmetric cell model is a very convenient way to simplify the problem, because it requires only two-dimensional calculations, so is the most frequently way to analyse the material behaviour. Those authors who only deal with axisymmetric conditions ignore the influence of other possible Lode parameter values in the response of the material. To analyse the influence of the Lode parameter, a cubic 3D cell in which a spherical void is contained should be considered (Zhang et al., 2001; Kim et al., 2007). In this paper, a unit cell with initial

lengths $2D_{01}$, $2D_{02}$ and $2D_{03}$ and a spherical void located at its center of radius r_0 is chosen. The RMV will be modelled by two approaches, one governed by the classical J_2 plasticity with a cell containing a discrete spherical void and another considering a homogeneous continuum damage model cell with the same initial void volume fraction as the voided one ($f_0 = \pi\, r_0^3/\,(6D_{01}D_{02}D_{03})$). Both cells are subjected to the same macroscopic loading history, obtained prescribing the displacements on the outer surfaces of each unitary cell. In both cases all boundaries are shear traction free, and the void surface in J_2 unit cell is also traction free, as shown in Fig. 1. Due to symmetry of the problem, only the eighth part of the region needs to be modelled.

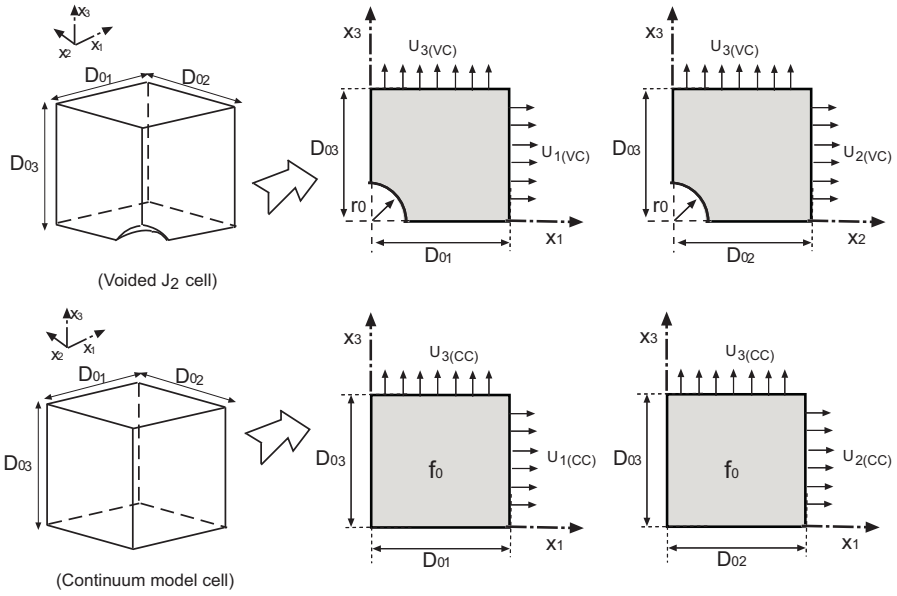

Figure 1: Geometry and displacements imposed as boundary conditions on the unitary J_2 voided cell and on the continuum damage model cell.

Assuming that the outer surfaces are always parallel to the 1, 2 and 3 directions respectively, the boundary conditions at the cell during the deformation process are:

$$\begin{aligned} u_1 &= 0 \quad \text{at } x_1 = 0; \qquad & u_1 &= U_1 \quad \text{at } x_1 = D_1; \\ u_2 &= 0 \quad \text{at } x_2 = 0; \qquad & u_2 &= U_2 \quad \text{at } x_2 = D_2; \\ u_3 &= 0 \quad \text{at } x_3 = 0; \qquad & u_3 &= U_3 \quad \text{at } x_3 = D_3; \end{aligned} \tag{1}$$

The macroscopic logaritmic principal strains have the form:

$$E_1 = \ln\left(\frac{D_1}{D_{01}}\right); \quad E_2 = \ln\left(\frac{D_2}{D_{02}}\right); \quad E_3 = \ln\left(\frac{D_3}{D_{03}}\right) \tag{2}$$

and the effective strain:

$$E_e = \frac{\sqrt{2}}{3}\left(\left(E_1 - E_2\right)^2 + \left(E_1 - E_3\right)^2 + \left(E_2 - E_3\right)^2\right)^{1/2} \tag{3}$$

with the rates of macroscopic logarithmic principal strains given by:

$$\dot{E}_1 = \frac{\dot{D}_1}{D_1}; \qquad \dot{E}_2 = \frac{\dot{D}_2}{D_2}; \qquad \dot{E}_3 = \frac{\dot{D}_3}{D_3} \tag{4}$$

where $D_1 = D_{01} + U_1$, $D_2 = D_{02} + U_2$ and $D_3 = D_{03} + U_3$ are the current lengths of the representative deformed cell.

The macroscopic principal stresses, Σ_1,Σ_2 and Σ_3 are defined as:

$$\Sigma_i = \frac{1}{D_j D_k}\int_0^{D_j}\int_0^{D_k} \left[\sigma_{ii}\right]_{x_i = D_i} dx_j dx_k \quad \text{with } i, j, k = 1, 2, 3$$

σ_{ii} being the Cauchy stress components, and Σ_e and Σ_h, the effective and hydrostatic macroscopic stresses:

$$\Sigma_e = \frac{1}{\sqrt{2}}\left(\left(\Sigma_1 - \Sigma_2\right)^2 + \left(\Sigma_1 - \Sigma_3\right)^2 + \left(\Sigma_2 - \Sigma_3\right)^2\right)^{1/2}; \qquad \Sigma_h = \frac{\Sigma_1 + \Sigma_2 + \Sigma_3}{3} \tag{5}$$

The stress triaxiality T and the Lode parameter L can be written as:

$$T = \frac{\Sigma_h}{\Sigma_e}; \quad \mathrm{L} = \frac{2\Sigma_2 - \Sigma_1 - \Sigma_3}{\Sigma_1 - \Sigma_3} \tag{6}$$

Defining the following ratios between Σ_1, Σ_2 and Σ_3:

$$R = \frac{\Sigma_2}{\Sigma_1}; \qquad Q = \frac{\Sigma_3}{\Sigma_1} \tag{7}$$

the stress triaxiality, T, and the Lode parameter, L, are given by:

$$T = \frac{\sqrt{2}\left(R + Q + 1\right)}{3\sqrt{\left(1 - R\right)^2 + \left(1 - Q\right)^2 + \left(R - Q\right)^2}}; \quad \mathrm{L} = \frac{2R - Q - 1}{1 - Q} \tag{8}$$

2.2. Boundary conditions for prescribing triaxiality and Lode parameters

In order to study the effect of stress triaxiality T and Lode parameter L in the mechanical behaviour of the representative volume element, boundary conditions should be implemented to prescribe the ratios of the principal stresses $R = \Sigma_2/\Sigma_1$ and $Q = \Sigma_3/\Sigma_1$ during the whole loading history of the RVE.

Faleskog et al. (1998) developed a method to prescribe displacement rates in a 3D unitary cell under plane strain condition which results in a constant macroscopic triaxiality. In this work, this strategy is extended to prescribe both triaxiality and Lode parameter during the entire deformation history of the 3D unitary cell.

In the voided J_2 cell, the macroscopic stresses Σ_i are calculated as the average stress on the cell boundaries. In the continuum damage model cell, Σ_i are the macroscopic stress in the prevailing homogeneous stress field. Since the macroscopic true stresses (Σ_1, Σ_2, Σ_3) and the macroscopic strain rates ($\dot{E}_1$, $\dot{E}_2$, $\dot{E}_3$) are equal to the volume average values in a cell (Hill, 1967), the total rate of deformation work $\dot{W}$ in both continuum damage model cell (CC) and J_2 voided cell (VC), can be written as:

$$\dot{W}_{CC} = \dot{W}_{VC} = V\Sigma_1\dot{E}_1 + V\Sigma_2\dot{E}_2 + V\Sigma_3\dot{E}_3 \tag{9}$$

V being the present volume of each cell.

Defining $P_1 = V\Sigma_1$, $P_2 = V\Sigma_2$ and $P_3 = V\Sigma_3$ as generalized forces and work rate conjugate quantities to $\dot{E}_1$, $\dot{E}_2$ and $\dot{E}_3$, respectively, the above expression becomes:

$$\dot{W}_{CC} = \dot{W}_{VC} = P_1\dot{E}_1 + P_2\dot{E}_2 + P_3\dot{E}_3 \tag{10}$$

in which the generalized forces P_1, P_2 and P_3 should satisfy, to prescribe the ratios of principal stresses $R = \Sigma_2/\Sigma_1$ and $Q = \Sigma_3/\Sigma_1$, the relations $P_2/P_1 = R$; $P_3/P_1 = Q$. Consider the transformation:

(11)

$$\begin{pmatrix} \dot{E}_{(I)} \\ \dot{E}_{(II)} \\ \dot{E}_{(III)} \end{pmatrix} = \mathbf{N} \begin{pmatrix} \dot{E}_1 \\ \dot{E}_2 \\ \dot{E}_3 \end{pmatrix}; \qquad \begin{pmatrix} P_{(I)} \\ P_{(II)} \\ P_{(III)} \end{pmatrix} = \mathbf{N} \begin{pmatrix} P_1 \\ P_2 \\ P_3 \end{pmatrix}$$

$\mathbf{N}$ being an orthonormal $\left(\mathbf{N}^{-1} = \mathbf{N}^{T}\right)$ unsymmetric matrix of the form:

$$\mathbf{N} = \begin{pmatrix} A_{11} & A_{12} & A_{13} \\ A_{21} & A_{22} & A_{23} \\ A_{31} & A_{32} & A_{33} \end{pmatrix};$$

with elements:

$$\begin{aligned} A_{11} &= \frac{1}{\sqrt{1+R^2+Q^2}}; \quad A_{12} = \frac{R}{\sqrt{1+R^2+Q^2}}; \quad A_{13} = \frac{Q}{\sqrt{1+R^2+Q^2}} \\ A_{21} &= -\frac{R}{\sqrt{1+R^2}}; \qquad A_{22} = \frac{1}{\sqrt{1+R^2}}; \qquad A_{23} = 0. \\ A_{31} &= \frac{Q}{\sqrt{(1+R^2)\,(1+R^2+Q^2)}}; \quad A_{32} = \frac{RQ}{\sqrt{(1+R^2)\,(1+R^2+Q^2)}} \\ A_{33} &= -\frac{(1+R^2)}{\sqrt{(1+R^2)\,(1+R^2+Q^2)}} \end{aligned} \tag{12}$$

The total rate of deformation work ($\dot{W}_{CC}$ and $\dot{W}_{VC}$) can be expressed as:

$$\dot{W}_{CC} = \dot{W}_{VC} = P_{(I)}\dot{E}_{(I)} + P_{(II)}\dot{E}_{(II)} + P_{(III)}\dot{E}_{(III)} \tag{13}$$

If in the transformed coordinate system, the imposed incremental boundary conditions are stress uniaxial:

$$\dot{E}_{(I)} = \dot{E}_I; \quad P_{(II)} = 0; \quad P_{(III)} = 0 \tag{14}$$

the total rate of deformation work has in this system the form $\dot{W}_{CC} = \dot{W}_{VC} = P_{(I)}\dot{E}_I$, that follows, in the original one and considering the relations given in Eqs. (11), the three relations:

$$\begin{aligned} &(1) \quad \dot{E}_{(I)} = \dot{E}_I \rightarrow \; A_{11}\dot{E}_1 + A_{12}\dot{E}_2 + A_{13}\dot{E}_3 = \dot{E}_I \\ &(2) \quad P_{(II)} = 0 \rightarrow \quad A_{21}P_1 + A_{22}P_2 + A_{23}P_3 = 0 \\ &(3) \quad P_{(III)} = 0 \rightarrow \quad A_{31}P_1 + A_{32}P_2 + A_{33}P_3 = 0 \end{aligned} \tag{15}$$

or in a similar manner:

$$\begin{aligned} &(1) \quad \dot{E}_1 + R\dot{E}_2 + Q\dot{E}_3 = \dot{E}_I\sqrt{1+R^2+Q^2} \\ &(2) \quad R\Sigma_1 = \Sigma_2 \\ &(3) \quad Q\Sigma_1 = \Sigma_3 \end{aligned} \tag{16}$$

For given values of R, Q and $\dot{E}_I$, imposing the three boundary conditions in the transformed system of each cell ($\dot{E}_{(I)} = \dot{E}_I$, $P_{(II)} = 0$, $P_{(III)} = 0$), lead to prescribe, in both continuum damage model cell (CC) and J_2 voided cell (VC) of the original system, the relations:

$$\begin{aligned} &(1) \quad \left(\dot{E}_1 + R\dot{E}_2 + Q\dot{E}_3\right)_{CC} = \left(\dot{E}_1 + R\dot{E}_2 + Q\dot{E}_3\right)_{VC} \\ &(2) \quad (\Sigma_2/\Sigma_1)_{CC} = (\Sigma_2/\Sigma_1)_{VC} = R \\ &(3) \quad (\Sigma_3/\Sigma_1)_{CC} = (\Sigma_3/\Sigma_1)_{VC} = Q \end{aligned} \tag{17}$$

with R and Q, from Eqs.(8) and for $\Sigma_3 < \Sigma_1$, as functions of T and L.

The boundary conditions are implemented in ABAQUS/Standard (Simulia, 2014) via a MPC subroutine. This method overcomes difficulties associated with cell softening due to void growth.

3. Numerical cell results for the voided J_2 and for the classical Gurson-Tvergaard model

Many authors (Zhang et al., 2001; Kim et al., 2007; Gao et al., 2005; Xue, 2008) show that a voided cell subjected to the same stress triaxiality ratio, would tends to react differently when Lode parameter is different. In this section, we will discuss the macroscopic stress-strain evolution and the growth of the porosity (until coalescence) of a voided J_2 cell subjected to prescribed triaxiality and Lode parameter values during the deformation history. For this purpose, the range of high stress triaxialities ($1 \leq T \leq 2$) and L values within the range ($-1 \leq L \leq 1$) are analyzed. The chosen material for the analysis is Weldox 960, material which presents a Lode parameter dependence behaviour as was experimentally proved by Barsoum et al. (2011). This high strength steel can be approximated by the following true stress-strain relation:

$$\sigma = \begin{cases} E\varepsilon & \varepsilon \leq \varepsilon_0 \\ \sigma_0 \left(\frac{\varepsilon}{\varepsilon_0}\right)^N & \varepsilon > \varepsilon_0 \end{cases} \tag{18}$$

where σ_0 represents the initial yield stress, N the strain hardening exponent and $\varepsilon_0 = \sigma_0/E$, E being the Young Modulus. All material properties are listed in Table 1.

It should be noted that at high triaxiality level, the prediction of ductile fracture depends on void growth, which is clearly different from the mechanism leading to failure at the low positive or negative hydrostratic stress fields (T values not considered in this work).

Table 1: Material properties of Weldox 960

E(GPa)	ν	σ_0 (MPa)	N	ε_0
208	0.3	956	0.059	0.0046

3.1. J_2 voided cell results

The RMV voided cell considered in this study has the initial length ratios $D_{01}/D_{02} = D_{01}/D_{03} = 1$, and two initial void volume fractions $f_0 = 0.005$ and $f_0 = 0.01$ are analyzed. The finite element mesh used in the calculations for $f_0 = 0.005$ is shown in Fig. 2, and consists of 8680 eight-node linear brick hexaedrical elements with reduced integration and hourglass control. This mesh includes 22 elements in the intersection of each outer surfaces with the void surface, and 20 elements along each longitudinal direction. The numerical analyses of the Weldox 960 material that obeys the theory of J_2 plasticity are carried out using the Finite Element code ABAQUS/Standard (Simulia, 2014) within an updated Lagrangian formulation. The nonlinear boundary conditions are prescribed following the method presented in previous section. Fig. 3 (a) illustrates the evolution of the

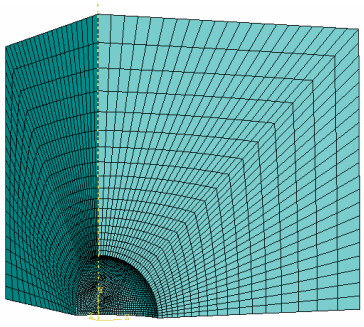

Figure 2: Example of the finite element mesh of a cell with initial void volume fraction $f_0 = 0.005$.

macroscopic effective stress versus effective strain curve for T=1, initial void volume fraction $f_0 = 0.005$ and Lode parameters $L = -1, -0.5, -0.2, 0, 0.2, 0.5, 1$. The competition between matrix material strain hardening and porosity induced softening is showed. As

macroscopic effective deformation increases, a maximum Σ_e/σ_0 value is reached, and the macroscopic effective stress decreases as strain-hardening of matrix material is insufficient to be balanced for a reduction in the cell ligament area caused by void expansion. When the Lode parameter has the minimum value (L=−1), the stress carrying capacity of the cell is reduced at lower E_e, whereas when L=1, the stress carrying capacity of the cell is lost much later (Zhang et al., 2001). The larger the L, the slower the lost of carrying capacity. The differences in the lost carrying capacity strongly depend of the evolution of the porosity f. As shown in Fig.3 (b), the larger the value of L tested, the smaller the increment of void volume fraction reached. Similar behaviour can be found for other high triaxialities tested.

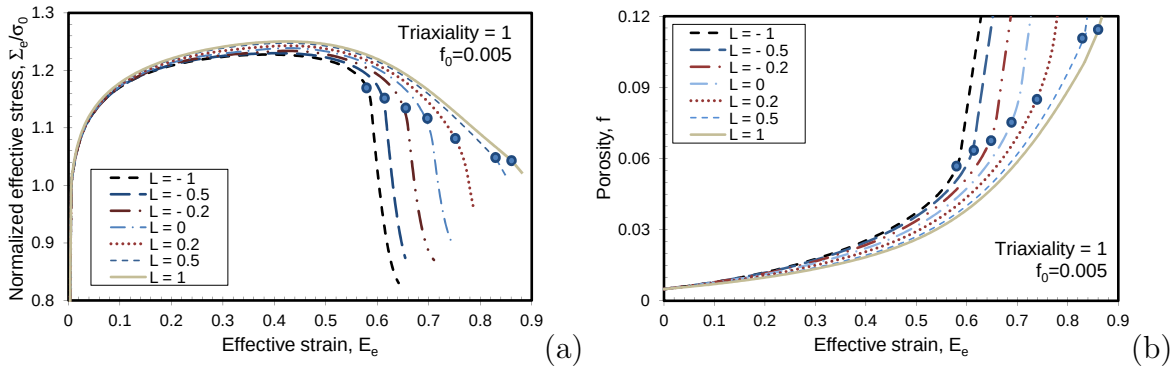

Figure 3: Evolution of macroscopic effective stress (a) and void volume fraction (b) versus macroscopic effective strain with different prescribed Lode parameters for $f_0 = 0.005$ and $T = 1$.

The rapid drop of stress carrying capacity and the fast increase of porosity f is marked with a circle in Fig. 3 (a) and (b) defining the onset of void coalescence. Following the procedure developed by Koplik and Needleman (1988) and Kim et al. (2004) for axisymmetric deformation mode, the evolution of ligament length ratios $(D_i - D_{i0})/D_{i0}$ in direction $i = 1,\ 2$ and 3 is represented as a function of E_e in Fig. 4 for $f_0 = 0.005$, T=1 and L=1, 0. The value of deformation where the evolution of ligament stretching stops in one (or two) directions and a rapid deformation in one (or two) directions take place, capture flow localization and the beginning of coalescence.

Not only void growth and critical strain for void instability are influenced by Lode parameter, also the expansion of the void can adopt different shapes for different L values under the same triaxiality level. It is well known that the influence of L on the deformation

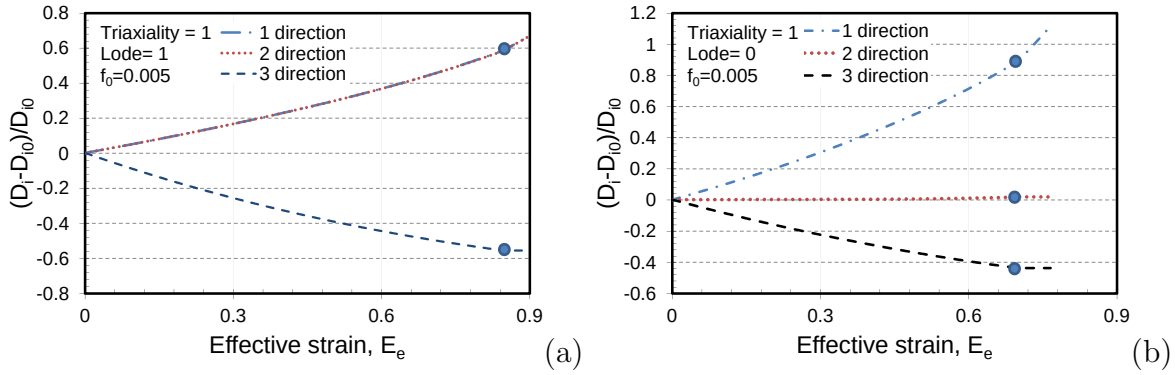

Figure 4: Variation of the deformed cell length ratio in directions i= 1, 2 and 3 vs. E_e for $f_0 = 0.005$, $T = 1$ and $L = 1,0$ revealing in each case a shift (circle) which corresponds to flow localization.

is more important at small values of T than at higher ones (Zhang et al., 2001). For high triaxialities, the shape of the voids remain nearly spherical for every L value analyzed.

3.2. Classical Gurson-Tvergaard cell results

The yield function of the Gurson-Tvergaard (GT) model has the form:

$$\Phi\left(\Sigma_e, \Sigma_h, \bar{\sigma}, f\right) = \frac{\Sigma_e^2}{\bar{\sigma}^2} + 2q_1 f cosh\left(\frac{3q_2\Sigma_h}{2\bar{\sigma}}\right) - \left(1 + q_1^2 f^2\right) \tag{19}$$

f being the current void volume fraction, $\bar{\sigma}$ the current flow stress of the matrix material, and Σ_e and Σ_h the effective and hydrostatic macroscopic Cauchy stresses:

$$\Sigma_e = \sqrt{\frac{3}{2}\boldsymbol{\Sigma}' : \boldsymbol{\Sigma}'} \quad ; \quad \Sigma_h = \frac{1}{3}\boldsymbol{\Sigma} : \mathbf{1} \quad ; \quad \boldsymbol{\Sigma}' = \boldsymbol{\Sigma} - \Sigma_h \mathbf{1} \tag{20}$$

The parameters q_1 and q_2 were introduced by Tvergaard (1981, 1982) to improve model predictions. The GT model does not capture the effect of the coalescence phase. The material behaviour in this phase prior to separation is not considered in this work.

The (q_1, q_2) Gurson-Tvergaard parameters strongly depend of material properties (Gao et al., 1998; Faleskog et al., 1998), and also are function of the initial void volume fraction f_0 and of the stress triaxiality ratio T (Kim et al., 2004; Vadillo and Fernández-Sáez, 2009). The proper selection of these two parameters are critical for the accurate representation of the ductile fracture of materials. The (q_1, q_2) values should be calibrated to match the stress-strain response and the void growth rate of the GT cell and that predicted by the J_2 voided cell analysis.

To minimize the differences between the two models, and for calibration purposes, two error functions are introduced, namely:

$$R_f = \frac{|F^I - F^{II}|}{F^I} \quad R_W = \frac{|W^I - W^{II}|}{W^I} \tag{21}$$

where F denotes the area under the curve of porosity f versus E_e, $\left(F = \int_0^{E_c} f dE_e\right)$, and W the area under the curve of the effective stress versus E_e, $\left(W = \int_0^{E_c} (\Sigma_e/\sigma_0) dE_e\right)$. E_c is the effective strain when coalescence is reached. Superscripts I and II refer to the voided cell and the GT model. $|F^I - F^{II}|$ and $|W^I - W^{II}|$ are respectively the areas between both curves in f vs. E_e and Σ_e vs. E_e schemes (blue zone in Figs. 5 (a) and (b))

Following Aravas (1987), a consistent integration procedure is used to integrate the GT model equations for Weldox 960. With the use of the backward Euler integration scheme, a numerical algorithm implicit in all variables is developed. The proposed algorithm as well as the corresponding tangent modulus is implemented in the Finite Element commercial code ABAQUS/Standard (Simulia, 2014) through a UMAT user subroutine.

It was already mentioned for the voided cell model that, in the case that both triaxiality and initial void volume fraction remain constant, the macroscopic stress-strain curves, the void growth rate and the coalescence strain differs markedly for every Lode parameter analyzed. In this work, and to calibrate GT parameters for fixed and constant T and f_0, the Lode parameter is chosen to be the one which gives earlier coalescence (L=-1) for all the cases tested.

For a given initial porosity, T and L, different pairs of (q_1, q_2) values give the same prediction for the error functions: R_f=TOL and R_W=TOL, with the chosen TOL= 0.01. Fig.5 (c) shows, for $f_0 = 0.005$, $T = 1$ and $L = -1$, the relations q_1-q_2 that minimize both R_f and R_W. The optimal choice for q_1, q_2 are obtained by the intersection of both curves. The q_1 and q_2 values are in this case q_1=0.855 and q_2=1.175.

A summary of the optimal GT parameters for two initial porosities $f_0 = 0.005$, $f_0 = 0.01$ and two different triaxialities 1 and 2 is given in Table 2. As mentioned, in all cases the chosen Lode parameter used for calibration purposes was $L = -1$. the coalescence strain E_c obtained from the voided cell and necessary for the calibration method is also given.

For simplicity, for the continuous field of triaxiality stress, $q_i(T)$ can be assumed to

vary following a linear function of the form (Vadillo and Fernández-Sáez, 2009):

$$q_i(T) = A_i\, T + B_i \tag{22}$$

with the interpolation coefficients A_i and B_i given in Table 2. Is a matter for discussion how to ensure yield surface convexity. Many authors test the convexity of the yield surface in a simple way, namely by plotting its two-dimensional projection at different loading stages (Pietryga et al., 2012). By taking advantage of this way, in the present work, convexity of the yield function is confirmed within the range of triaxialities $1 \leq T \leq 2$ and $L = -1$ for porosities $f_0 \leq f \leq 0.08$ for the initial void volume fractions $f_0 = 0.005$ and 0.01.

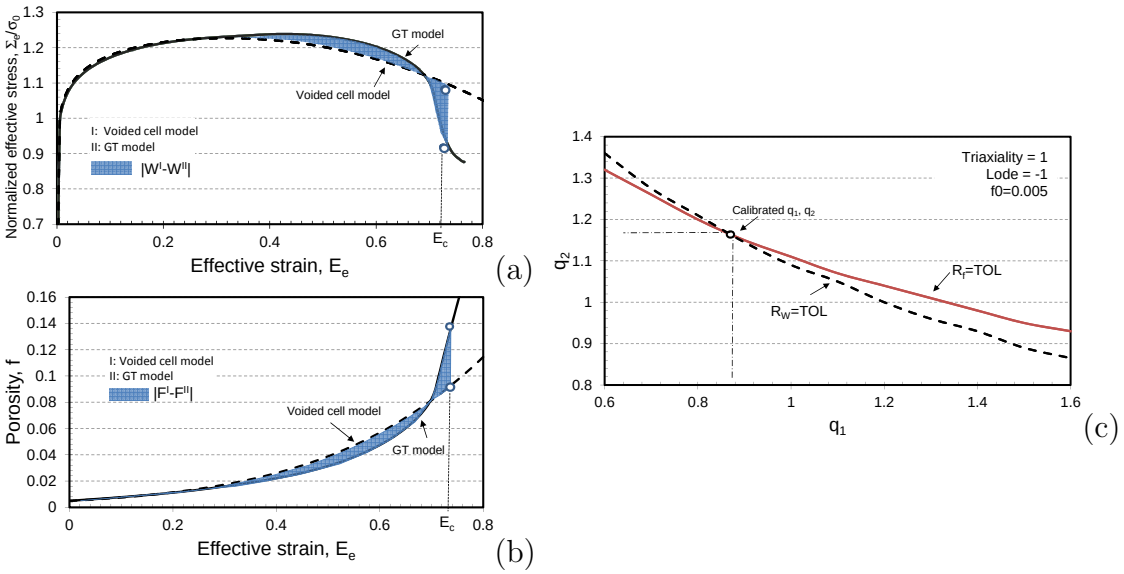

Figure 5: Fitting squemes for Σ_e vs. E_e and f vs. E_e, (a) and (b), and example of calibration procedure for q_1 and q_2 parameters for $f_0 = 0.005$, $T = 1$ and $L = -1$ (c).

Table 2: Optimal q_1, q_2 and E_c for $T = 1, 2$, and interpolation coefficients of $q_i(T)$ for $f_0 = 0.005$ and 0.01.

	$f_0 = 0.005$			$f_0 = 0.01$	
T	1	2		1	2
q_1	0.855	1.455		1.011	1.583
q_2	1.175	0.992		1.104	0.957
E_c	0.580	0.160		0.480	0.130

	$q_1(T)$			$q_2(T)$	
f_0	A_1	B_1		A_2	B_2
0.005	0.600	0.255		-0.183	1.358
0.01	0.572	0.439		-0.147	1.251

Fig.6 compares the evolution of macroscopic stress-strain and the predicted void-volume fraction growth till coalescence using GT model with calibrated q_i parameters (Table 2) using the results of the J_2 voided cell model. The cases analyzed corresponds to f_0=0.005, $T = 1$, 2 and L= -1, 0 and 1. It can be seen how the classical GT model, Lode independent, predicts the same behavior for different stress states when the triaxiality ratio is the same, meanwhile voided J_2 cell response differs when Lode parameter changes. It is observed, for every triaxiality studied, how the difference between the two models increase when the value of the Lode parameter increases.

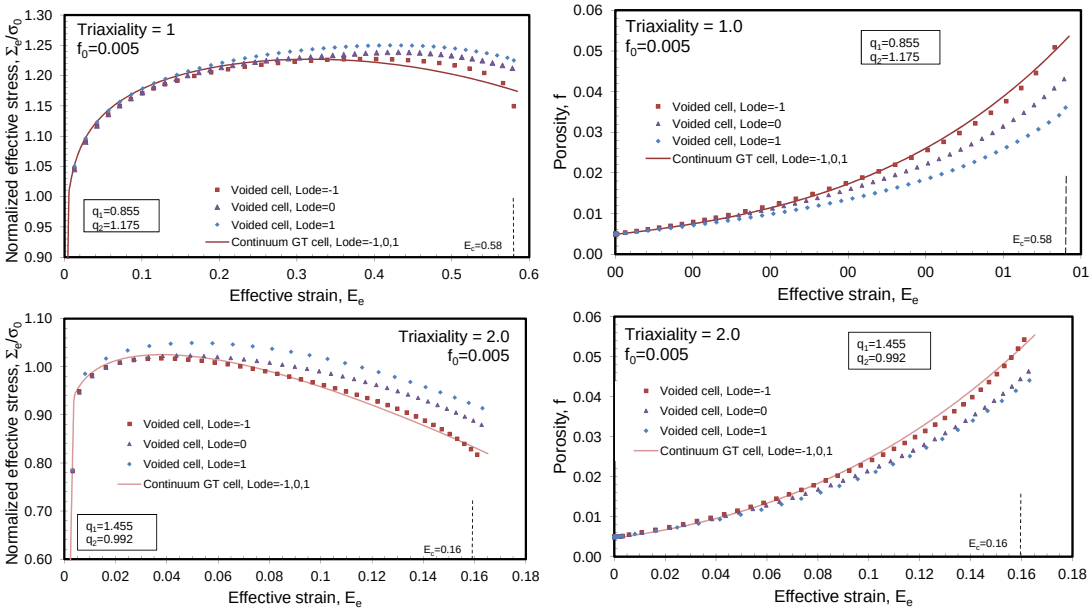

Figure 6: Comparison of Σ_e vs. E_e curve and f vs. E_e curve for a voided cell and a continuum GT cell with different calibrated q_i parameters. Here, f_0=0.005, T=1, 2 and L=-1, 0, 1.

4. Modified Gurson-Tvergaard model with Lode parameter dependence

4.1. Constitutive equations

One of the major limitations of the GT model is that, although it is extensively used, it can only handle the growth of spherical voids remaining spherical, which is only aproximately true for L =-1 and at triaxialities around 1.5. However, at high triaxialities, it is possible to calibrate q_1 and q_2 parameters in GT model to reproduce the behavior of the material in these stress situations. These calibrated q_i values are not constants, but

dependent on the material, the stress triaxiality ratio and the initial void volume fraction considered (Kim et al., 2004; Vadillo and Fernández-Sáez, 2009).

J_2 cell model analysis conducted in previous sections show that the macroscopic stress-strain response and the void growth behaviour not only depend on the first and the second stress invariants, but also on the Lode parameter (third stress invariant). However, the original GT model predicts the same void growth rate and macroscopic stress-strain response for different Lode parameter values as long as the stress triaxiality ratio T remains the same.

At low triaxialities (Nahshon and Hutchinson, 2008) have proposed a modification of the Gurson model to capture softening in shear. The modification takes into account the third invariant of the stress deviator.

At high triaxialities, and in order to account for the influence of T and L on the response of the material, the main innovative feature of this work is to propose a modification of the yield function of the classical GT model (Eq. (19)) introducing new dependences in q_1 and q_2 Gurson-Tvergaard parameters as functions of triaxiality and Ω. The proposed yield function has the form:

$$\Phi_{mod}\left(\Sigma_e, \Sigma_h, T, \Omega, \bar{\sigma}, f\right) = \frac{\Sigma_e^2}{\bar{\sigma}^2} + 2q_{1mod} f cosh\left(\frac{3q_{2mod}\Sigma_h}{2\bar{\sigma}}\right) - \left(1 + \left(q_{1mod}\right)^2 f^2\right) \tag{23}$$

with q_{1mod}, q_{2mod}, for the sake of simplicity, defined as linear functions of T and Ω as:

$$q_{1mod}(T, \Omega) = q_1(T) \cdot (1 + k_\Omega \cdot \Omega); \tag{24}$$

$$q_{2mod}(T, \Omega) = q_2(T) \cdot (1 + k_\Omega \cdot \Omega) \tag{25}$$

The functions $q_1(T)$ and $q_2(T)$ in q_{1mod} and q_{2mod} follows (Eq. 22) with A_i and B_i interpolated coefficients based of fitted discrete q_i values obtained from the axisymmetric stress state field ($\Omega = 0$). Ω is a stress measure, function of the effective stress Σ_e and J_3 as:

$$\Omega = \frac{27 J_3}{2\Sigma_e^3} - 1; \quad J_3 = \det(\mathbf{\Sigma}')$$

lying in the range $-2 \leq \Omega \leq 0$, with $\Omega = 0$ for $L = -1$, and $\Omega = -2$ for $L = 1$. k_Ω is a proposed adjustment parameter. This modification is purely phenomenological, but formulated to retrieve the original GT formulation for $L = -1$ and T=constant.

For hypoelastic-plastic materials, the relation between the macroscopic stress rate, $\dot{\mathbf{\Sigma}}$, and the plastic part of the rate of macroscopic deformation $\dot{\mathbf{E}}^p$ is given by:

$$\dot{\mathbf{\Sigma}} = \mathbf{C} : \left(\dot{\mathbf{E}} - \dot{\mathbf{E}}^p\right) \tag{26}$$

$\dot{\mathbf{E}}$ being the macroscopic rate of deformation tensor and $\mathbf{C} = 2G\mathbf{I}' + K\mathbf{1}\otimes\mathbf{1}$ the fourth-order tensor of isotropic elastic moduli. G and K are the Shear and Bulk modulus respectively, $\mathbf{I}'$ the unit deviatoric fourth order tensor and $\mathbf{1}$ the unit second order tensor.

The plastic part of the rate of macroscopic deformation $\dot{\mathbf{E}}^p$ is derived from the associated flow rule:

$$\dot{\mathbf{E}}^p = \dot{\lambda}\frac{\partial \Phi_{mod}}{\partial \mathbf{\Sigma}} \tag{27}$$

$\dot{\lambda}$ being the plastic flow proportionality factor, and Φ_{mod} the GT yield condition modified in this work to take into account the influence of the Lode parameter on the ductile behaviour of elasto-plastic porous materials.

The plastic part of the macroscopic strain rate and the effective plastic strain rate are related by enforcing equality between the rates of macroscopic and matrix plastic work:

$$\mathbf{\Sigma} : \dot{\mathbf{E}}^p = (1-f)\,\bar{\sigma}\dot{\bar{\varepsilon}}^p \tag{28}$$

Here, the flow stress of the matrix material $\bar{\sigma}$ and the effective microscopic plastic strain rate $\dot{\bar{\varepsilon}}^p$ are related by the law $\bar{\sigma} = \bar{\sigma}\left(\bar{\varepsilon}^p\right)$ with $\bar{\varepsilon}^p = \int_0^t \dot{\bar{\varepsilon}}^p(\tau)d\tau$,

The evolution of porosity can be written as:

$$\dot{f} = (1-f)\dot{\mathbf{E}}^p : \mathbf{1} \tag{29}$$

One should note that the evolution law for the void volume fraction is affected by the definition of the yield surface, having a dependence with Lode parameter as far as the yield function does.

The above formulation must be complemented with the Kuhn-Tucker conditions:

$$\dot{\lambda} \geq 0, \quad \Phi_{mod} \leq 0, \quad \dot{\lambda}\Phi_{mod} = 0 \tag{30}$$

and the consistency condition during plastic loading: $\dot{\Phi}_{mod} = 0$

5. Numerical implementation

5.1. Integration procedure

In the context of the Finite-Element method, the integration process is local in space and occurs at each quadrature points of the finite elements. The incremental integration of the constitutive equations is a strain-driven process in which the total strain tensor increment at each quadrature point, $\dot{\mathbf{E}}$, is given at a time (n) and both the stress tensor and the state variables should be updated at time (n+1).

To integrate the set of non-linear constitutive Eqs. (26-30) , two different tasks must be accomplished. The first one consists in update stress and state variables driven by the strain increment. The second is related to define a consistent tangent modulus to preserve the quadratic convergence of the iterative solution based on Newton's method. All variables are evaluated in $(n+1)$, omitting the subscript for simplicity.

For the first assignment, the classical return mapping algorithm is used (Simo and Taylor, 1985). Following a fully Backward-Euler scheme, the constitutive relations can be written in the following incremental form:

- From the time derivative of the generalized Hooke's law (Eq. (26)):

$$\boldsymbol{\Sigma} = \boldsymbol{\Sigma}^{trial} - \mathbf{C} : \boldsymbol{\Delta}\mathbf{E}^p \quad \text{with} \quad \boldsymbol{\Sigma}^{trial} = \boldsymbol{\Sigma}_{(n)} + \mathbf{C} : \boldsymbol{\Delta}\mathbf{E} \tag{31}$$

- From the flow rule (Eq. (27)):

$$\boldsymbol{\Delta}\mathbf{E}^p = \Delta\lambda \frac{\partial \Phi_{mod}}{\partial \boldsymbol{\Sigma}} = \Delta\lambda \left(\frac{1}{3} \left(\frac{\partial \Phi_{mod}}{\partial \Sigma_h} + \frac{\partial \Phi_{mod}}{\partial T} \frac{\partial T}{\partial \Sigma_h} \right) \mathbf{1} + \right. \tag{32}$$
$$\left. + \left(\frac{\partial \Phi_{mod}}{\partial \Sigma_e} + \frac{\partial \Phi_{mod}}{\partial T} \frac{\partial T}{\partial \Sigma_e} \right) \frac{3\boldsymbol{\Sigma}'}{2\Sigma_e} + \frac{\partial \Phi_{mod}}{\partial \Omega} \frac{\partial \Omega}{\partial \boldsymbol{\Sigma}} \right)$$

  with

$$\frac{\partial \Omega}{\partial \boldsymbol{\Sigma}} = -\frac{81}{2} \frac{J_3}{\Sigma_e^4} \cdot \frac{3}{2} \frac{\boldsymbol{\Sigma}'}{\Sigma_e} + \frac{27}{2\Sigma_e^3} \left(\operatorname{cof}(\boldsymbol{\Sigma}') + \frac{1}{9}\Sigma_e^2 \mathbf{1} \right) \tag{33}$$

  $\mathbf{1}$ being the unit second-order tensor, and $(\operatorname{cof}(\boldsymbol{\Sigma}'))_{ij} = \frac{1}{2} e_{jkr} e_{ist} (\boldsymbol{\Sigma}')_{sk} (\boldsymbol{\Sigma}')_{tr}$ the minors of $(\boldsymbol{\Sigma}')$, with e_{ijk} the Levi-Civita permutation symbols which allow the flow rule dependent on Ω to be written as:

$$\boldsymbol{\Delta}\mathbf{E}^p = \Delta\lambda \frac{\partial \Phi_{mod}}{\partial \boldsymbol{\Sigma}} = \frac{1}{3}\Delta\varepsilon_p \mathbf{1} + \Delta\varepsilon_q \frac{3\boldsymbol{\Sigma}'}{2\Sigma_e} + \Delta\varepsilon_\Omega \frac{\partial \Omega}{\partial \boldsymbol{\Sigma}} \tag{34}$$

being $\Delta\varepsilon_p$, $\Delta\varepsilon_q$ and $\Delta\varepsilon_\Omega$ in the form:

$$\begin{aligned}\Delta\varepsilon_p &= \Delta\lambda\left(\frac{\partial\Phi_{mod}}{\partial\Sigma_h}+\frac{\partial\Phi_{mod}}{\partial T}\frac{\partial T}{\partial\Sigma_h}\right)\\ \Delta\varepsilon_q &= \Delta\lambda\left(\frac{\partial\Phi_{mod}}{\partial\Sigma_e}+\frac{\partial\Phi_{mod}}{\partial T}\frac{\partial T}{\partial\Sigma_e}\right)\\ \Delta\varepsilon_\Omega &= \Delta\lambda\left(\frac{\partial\Phi_{mod}}{\partial\Omega}\right)\end{aligned} \tag{35}$$

that leads, after combining the above relations to eliminate $\Delta\lambda$:

$$\begin{aligned}&\Delta\varepsilon_p\left(\frac{\partial\Phi_{mod}}{\partial\Sigma_e}+\frac{\partial\Phi_{mod}}{\partial T}\frac{\partial T}{\partial\Sigma_e}\right)-\Delta\varepsilon_q\left(\frac{\partial\Phi_{mod}}{\partial\Sigma_h}+\frac{\partial\Phi_{mod}}{\partial T}\frac{\partial T}{\partial\Sigma_h}\right)=0;\\ &\Delta\varepsilon_q\frac{\partial\Phi_{mod}}{\partial\Omega}-\Delta\varepsilon_\Omega\left(\frac{\partial\Phi_{mod}}{\partial\Sigma_e}+\frac{\partial\Phi_{mod}}{\partial T}\frac{\partial T}{\partial\Sigma_e}\right)=0\end{aligned} \tag{36}$$

Taking into account the identity:

$$\boldsymbol{\Sigma}' : \mathrm{cof}\,(\boldsymbol{\Sigma}'\,) = 3J_3 \tag{37}$$

it is possible to prove that the product $\boldsymbol{\Sigma}' : \frac{\partial\Omega}{\partial\boldsymbol{\Sigma}}$ is equal to zero allowing the constitutive relations to be written as:

- Macroscopic and matrix plastic work equivalence: $\Sigma_h\Delta\varepsilon_p+\Sigma_e\Delta\varepsilon_q=(1-f)\bar{\sigma}\Delta\bar{\varepsilon}^p$
- Void volume fraction evolution equation:$\Delta f=(1-f)\,\Delta\varepsilon_p$
- Kuhn-Tucker condition for plastic loading: $\Delta\Phi_{mod}=0$

Substituting Eq. (34) into the deviatoric part of Eq. (31), the updated deviatoric stress has the form:

$$\boldsymbol{\Sigma}' = \boldsymbol{\Sigma}'^{\,trial}-3G\Delta\varepsilon_q\frac{\boldsymbol{\Sigma}'}{\Sigma_e}-2G\Delta\varepsilon_\Omega\left(-\frac{81}{2}\frac{J_3}{\Sigma_e^4}\cdot\frac{3}{2}\frac{\boldsymbol{\Sigma}'}{\Sigma_e}+\frac{27}{2\Sigma_e^3}\left(\mathrm{cof}\,(\boldsymbol{\Sigma}')+\frac{1}{9}\Sigma_e^2\mathbf{1}\right)\right) \tag{38}$$

with

$$\boldsymbol{\Sigma}'^{\,trial}=\boldsymbol{\Sigma}'_{(n)}+2G\mathbf{I}':\boldsymbol{\Delta}\mathbf{E} \tag{39}$$

where $\boldsymbol{\Sigma}'$ can be written in the form:

$$X\boldsymbol{\Sigma}'=\boldsymbol{\Sigma}'^{\,trial}-Y\mathrm{cof}\left(\boldsymbol{\Sigma}'\right)-Z\mathbf{1}; \tag{40}$$

with X, Y and Z given by:

$$X = 1 + \frac{3G}{\Sigma_e}\Delta\varepsilon_q - \frac{243\ G\ J_3}{2\Sigma_e^5}\Delta\varepsilon_\Omega;\ \ Y = \frac{27G}{\Sigma_e^3}\Delta\varepsilon_\Omega;\quad Z = \frac{\Sigma_e^2\ Y}{9}; \tag{41}$$

and $\mathrm{cof}\,(\boldsymbol{\Sigma}')$, computing it from the expression given in Eq.(40), as:

$$(X^2 - YZ)\mathrm{cof}\left(\boldsymbol{\Sigma}'\right) = \mathrm{cof}\left(\boldsymbol{\Sigma}'^{trial}\right) - \left(2XZ + Y^2 J_3\right)\boldsymbol{\Sigma}' + \left(XYJ_3 + 2Z^2\right)\mathbf{1} \tag{42}$$

From Eq. (38), and after some algebra taking into account the identities:

$$\mathrm{cof}\,(\boldsymbol{\Sigma}'\,) : \mathrm{cof}\,(\boldsymbol{\Sigma}'\,) = \frac{\Sigma_e^4}{9},\ \ \mathrm{cof}\,(\boldsymbol{\Sigma}'\,) : \mathbf{1} = -\frac{\Sigma_e^2}{3} \tag{43}$$

the following relations between the trial and current stress measures can be found-see Appendix A:

$$\left(\Sigma_e^{trial}\right)^2 = \left(\Sigma_e + 3G\Delta\varepsilon_q\right)^2 + \left(\frac{9G\Delta\varepsilon_\Omega}{\Sigma_e}\right)^2\left(1 - (\Omega+1)^2\right) \tag{44}$$

$$J_3^{trial} = \frac{2\Sigma_e^3}{27}\left[(\Omega+1)\,X^3 + \frac{\left(Y\Sigma_e\right)^3}{27}\left(2\,(\Omega+1)^2 - 1\right) + X^2\,(Y\Sigma_e) + \frac{(\Omega+1)\,X}{3}\,(Y\Sigma_e)^2\right]$$

with $\Sigma_e^{trial} = \sqrt{\frac{3}{2}\boldsymbol{\Sigma}'^{trial} : \boldsymbol{\Sigma}'^{trial}}$, $\ J_3^{trial} = \det(\boldsymbol{\Sigma}'^{\ trial})$, and

$$X = 1 + \frac{3G}{\Sigma_e}\Delta\varepsilon_q - \frac{9\ G\ (\Omega+1)}{\Sigma_e^2}\Delta\varepsilon_\Omega;\qquad Y = \frac{27G}{\Sigma_e^3}\Delta\varepsilon_\Omega; \tag{45}$$

In a similar manner, it can be easily proved the relation:

$$\Sigma_h^{trial} = \Sigma_h + K\Delta\varepsilon_p \tag{46}$$

The set of five non-linear equations, involving only scalars, that should be solved to obtain the five unknown variables $\Delta\varepsilon_p$, $\Delta\varepsilon_q$, $\Delta\varepsilon_\Omega$, f and $\bar{\varepsilon}^p$ using an iterative Newton-Raphson procedure, are:

$$\Delta\varepsilon_p\left(\frac{\partial\Phi_{mod}}{\partial\Sigma_e} + \frac{\partial\Phi_{mod}}{\partial T}\frac{\partial T}{\partial\Sigma_e}\right) - \Delta\varepsilon_q\left(\frac{\partial\Phi_{mod}}{\partial\Sigma_h} + \frac{\partial\Phi_{mod}}{\partial T}\frac{\partial T}{\partial\Sigma_h}\right) = 0; \tag{47}$$

$$\Delta\varepsilon_q\frac{\partial\Phi_{mod}}{\partial\Omega} - \Delta\varepsilon_\Omega\left(\frac{\partial\Phi_{mod}}{\partial\Sigma_e} + \frac{\partial\Phi_{mod}}{\partial T}\frac{\partial T}{\partial\Sigma_e}\right) = 0$$

$$\Sigma_h\Delta\varepsilon_p + \Sigma_e\Delta\varepsilon_q = (1-f)\bar{\sigma}\Delta\bar{\varepsilon}^p$$

$$\Delta f = (1-f)\Delta\varepsilon_p$$

$$\Phi_{mod}\left(\Sigma_e, \Sigma_h, T, \Omega, \bar{\sigma}, f\right) = 0$$

with $\bar{\sigma} = \bar{\sigma}(\bar{\varepsilon}^p)$, and Σ_h, Σ_e and Ω obtained from the relations:

$$\Sigma_h = \Sigma_h^{trial} - K\Delta\varepsilon_p \tag{48}$$
$$\left(\Sigma_e + 3G\Delta\varepsilon_q\right)^2 + \left(\frac{9G\Delta\varepsilon_\Omega}{\Sigma_e}\right)^2 \left(1 - (\Omega+1)^2\right) = \left(\Sigma_e^{trial}\right)^2$$
$$\frac{2\Sigma_e^3}{27}\left[(\Omega+1)\,X^3 + \frac{(Y\Sigma_e)^3}{27}\left(2\,(\Omega+1)^2 - 1\right) + X^2\,(Y\Sigma_e) + \frac{(\Omega+1)\,X}{3}\,(Y\Sigma_e)^2\right] = J_3^{trial}$$

and X and Y given by Eq. (45).

Once the set of equations Eq.(47) are solved, Eqs.(40) and (42) allows ($\mathbf{\Sigma}'$) to be written as function of $\mathbf{1}$ and the trial tensors $\mathbf{\Sigma}'^{trial}$ and cof $\left(\mathbf{\Sigma}'^{trial}\right)$.

Finally, the updated stress $\mathbf{\Sigma}$ at time (n+1) can be calculated as $\mathbf{\Sigma} = \Sigma_h\mathbf{1} + \mathbf{\Sigma}'$.

5.2. Consistent tangent modulus

For infinitesimal strain problems, Simo and Taylor (1985) showed that the use of a consistent tangent modulus $\mathbf{J}$ preserves the quadratic rate of asymptotic convergence of iterative solution schemes based on the Newton's method. This tangent operator defines the variation in stress at time (n+1) caused by a variation of the total strain as:

$$\mathbf{J} = \left(\frac{\partial\mathbf{\Sigma}}{\partial\mathbf{E}}\right)_{(n+1)} \tag{49}$$

For classical Gurson materials, an explicit expression of the tangent modulus consistent with the Euler backward algorithm has been given by (Aravas, 1987; Zhang, 1995; Vadillo and Fernández-Sáez, 2009). Following this procedure, the consistent stiffness matrix for the modified GT model proposed in this work, J_3 dependent, is obtained as follows (since all quantities in calculating $\mathbf{J}$ are referred to time (n+1), the superscript (n+1) will be dropped hereafter). For the convenience of the finite element implementation, $\mathbf{J}$ will be derived in matrix form. The boldface symbols will be used to denote matrices and vectors where:

$$\boldsymbol{\partial\Sigma} = \{\partial\Sigma_{11}, \partial\Sigma_{22}, \partial\Sigma_{33}, \partial\Sigma_{12}, \partial\Sigma_{13}, \partial\Sigma_{23}, \partial\Sigma_{21}, \partial\Sigma_{31}, \partial\Sigma_{32}\}^T \tag{50}$$
$$\boldsymbol{\partial\mathbf{E}} = \{\partial E_{11}, \partial E_{22}, \partial E_{33}, \partial E_{12}, \partial E_{13}, \partial E_{23}, \partial E_{21}, \partial E_{31}, \partial E_{32}\}^T$$

Deriving Eqs. (31) considering the relation given in Eq. (46):

$$\boldsymbol{\partial\Sigma} \;\; = \partial\Sigma_h\mathbf{1} + \boldsymbol{\partial\Sigma'} = \partial\Sigma_h^{trial}\mathbf{1} - K\partial\Delta\varepsilon_p\mathbf{1} + \boldsymbol{\partial\Sigma'} \tag{51}$$

Deriving Eq. (40):

$$\boldsymbol{\Sigma'}\,\partial X + X\,\boldsymbol{\partial \Sigma'} = \boldsymbol{\partial \Sigma'}^{trial} - \partial Y \mathrm{cof}\,(\boldsymbol{\Sigma'}) - Y\boldsymbol{\partial}\,(\mathrm{cof}\boldsymbol{\Sigma'}) - \partial Z\mathbf{1}; \tag{52}$$

$\mathbf{1}$ and $\mathbf{I}'$ being the vector and matrix mapping of the unit second order tensor and the unit deviatoric fourth-order tensor respectively.

∂X, ∂Y and ∂Z are functions of $\partial\Sigma_h^{trial}$, $\partial\Sigma_e^{trial}$ and ∂J_3^{trial} -see Eqs.(B.4a, B.7, B.9) from Appendix B. $\mathrm{cof}\,(\boldsymbol{\Sigma'})$ and $\boldsymbol{\partial}\,(\mathrm{cof}\boldsymbol{\Sigma'})$ are functions of $\boldsymbol{\Sigma'}^{trial}$ and $\mathrm{cof}\left(\boldsymbol{\Sigma'}^{\,trial}\right)$-see Eqs.(42) and Eq.(B.11). Taking into account these relations, and clearing $\boldsymbol{\partial\Sigma'}$ from Eq.(52) we have:

$$\boldsymbol{\partial \Sigma'} = \boldsymbol{\partial \Sigma'}^{trial} + \tilde{E}_1 \boldsymbol{\Sigma'}^{trial} + \tilde{E}_2 \mathrm{cof}\left(\boldsymbol{\Sigma'}^{\,trial}\right) + \tilde{E}_3\mathbf{1} + F\boldsymbol{\partial}\left(\mathrm{cof}\boldsymbol{\Sigma'}^{trial}\right) \tag{53}$$

with $\tilde{E}_1$, $\tilde{E}_2$ and $\tilde{E}_3$ of the form:

$$\tilde{E}_i = \tilde{E}_{i1}\partial\Sigma_h^{trial} + \tilde{E}_{i2}\partial\Sigma_e^{trial} + \tilde{E}_{i3}\partial J_3^{trial} \tag{54}$$

being all coefficients $\tilde{E}_{ij}$ and F known.

Introducing the relation (see Appendix B):

$$\partial\Delta\varepsilon_p \;=\; \tilde{B}_{11}\partial\Sigma_h^{trial} + \tilde{B}_{12}\partial\Sigma_e^{trial} + \tilde{B}_{13}\partial J_3^{trial} \tag{55}$$

and the identities:

$$\begin{aligned}
&\partial\Sigma_h^{trial} = K\,(\mathbf{1})^T \cdot \boldsymbol{\partial}\mathbf{E} \\
&\partial\Sigma_e^{trial} = \frac{3}{2\Sigma_e^{trial}}\left(\boldsymbol{\Sigma'}^{\,trial}\right)^T \cdot \boldsymbol{\partial\Sigma'}^{\,trial} \\
&\partial J_3^{trial} = \left(\mathrm{cof}\left(\boldsymbol{\Sigma'}^{\,trial}\right)\right)^T \cdot \boldsymbol{\partial\Sigma'}^{\,trial} \\
&\boldsymbol{\partial\Sigma'}^{\,trial} = 2G\mathbf{I}' \cdot \boldsymbol{\partial}\mathbf{E} \\
&\boldsymbol{\partial}\left(\mathrm{cof}\left(\boldsymbol{\Sigma'}^{\,trial}\right)\right) = \mathbf{M} \cdot \boldsymbol{\partial\Sigma'}^{\,trial}
\end{aligned} \tag{56}$$

where $\mathbf{M}$ is a 9x9 matrix of the form:

$$\mathbf{M} = \begin{bmatrix} 0 & \Sigma_{33}^{trial} & \Sigma_{22}^{trial} & 0 & 0 & -\Sigma_{32}^{trial} & 0 & 0 & -\Sigma_{23}^{trial} \\ \Sigma_{33}^{trial} & 0 & \Sigma_{11}^{trial} & 0 & -\Sigma_{31}^{trial} & 0 & 0 & -\Sigma_{13}^{trial} & 0 \\ \Sigma_{22}^{trial} & \Sigma_{11}^{trial} & 0 & -\Sigma_{21}^{trial} & 0 & 0 & -\Sigma_{12}^{trial} & 0 & 0 \\ 0 & 0 & -\Sigma_{21}^{trial} & 0 & 0 & \Sigma_{31}^{trial} & -\Sigma_{33}^{trial} & \Sigma_{23}^{trial} & 0 \\ 0 & -\Sigma_{31}^{trial} & 0 & 0 & 0 & 0 & \Sigma_{32}^{trial} & -\Sigma_{22}^{trial} & \Sigma_{21}^{trial} \\ -\Sigma_{32}^{trial} & 0 & 0 & \Sigma_{31}^{trial} & 0 & 0 & 0 & \Sigma_{12}^{trial} & -\Sigma_{11}^{trial} \\ 0 & 0 & -\Sigma_{12}^{trial} & -\Sigma_{33}^{trial} & \Sigma_{32}^{trial} & 0 & 0 & 0 & \Sigma_{13}^{trial} \\ 0 & -\Sigma_{13}^{trial} & 0 & \Sigma_{23}^{trial} & -\Sigma_{22}^{trial} & \Sigma_{12}^{trial} & 0 & 0 & 0 \\ -\Sigma_{23}^{trial} & 0 & 0 & 0 & \Sigma_{21}^{trial} & -\Sigma_{11}^{trial} & \Sigma_{13}^{trial} & 0 & 0 \end{bmatrix} \tag{57}$$

into Eq. (51), the tangent modulus $\mathbf{J}$ can be written as:

$$\begin{aligned} \mathbf{J} &= K\left(1 - K\tilde{B}_{11} + \tilde{E}_{31}\right)\mathbf{1}\cdot\mathbf{1}^T + K\tilde{E}_{21}\ \cdot \mathrm{cof}\left(\boldsymbol{\Sigma}'^{\,trial}\right)\cdot\mathbf{1}^{\,T} + \\ &+\frac{3G}{\Sigma_e^{trial}}\left(\tilde{E}_{12}\boldsymbol{\Sigma}'^{\,trial} + \tilde{E}_{22}\mathrm{cof}\left(\boldsymbol{\Sigma}'^{\,trial}\right)\right)\cdot\left(\boldsymbol{\Sigma}'^{\,trial}\right)^T + \\ &+2G\left(\tilde{E}_{13}\boldsymbol{\Sigma}'^{\,trial} + \tilde{E}_{23}\mathrm{cof}\left(\boldsymbol{\Sigma}'^{\,trial}\right)\right)\cdot\mathbf{I}'\cdot\mathrm{cof}\left(\boldsymbol{\Sigma}'^{\,trial}\right)^T + 2G\left(\mathbf{I}' + F\cdot\mathbf{M}\cdot\mathbf{I}'\right) \end{aligned} \tag{58}$$

To define this operator is not required any matrix inversion. The described algorithm as well as the corresponding tangent modulus has been implemented in the commercial finite element code ABAQUS/Standard (Simulia, 2014) through the user subroutine UMAT.

6. Comparison between the voided J_2 cell and the modified continuum GT cell

In order to analyse the accuracy of the proposed model, a selection of different loading and initial void volume fractions for Weldox 960 material will be studied in this section. The stress-strain and void volume fraction evolution within the deformation range $0 \leq E_e \leq E_c$ have been compared for the two RVE cell model approaches using three different triaxiality values ($T = 1, 1.5, 2$) and two Lode parameters ($L = 0, 1$) for the initial porosities f_0=0.005 and f_0=0.01. The case corresponding with $L = -1$ should not be analysed in the sense that for this Lode value the modified GT model coincides with the classical GT model and the behaviour of GT and J_2 voided cell are essentially the same as far as the q_i parameters used for simulations were calibrated to minimize these differences.

After a numerical iterative analysis, for the most critical stress and void volume fraction situations found in this work ($f \leq 0.08$), convexity is assured if $0 \leq k_\Omega \leq 0.0403$.

Results for T= 1 and L= 0 are shown in Figs. 7 for $f_0 = 0.005$ (a)-(b) and $f_0 = 0.01$ (c)-(d) considering the J_2 voided cell (dotted line) and the continuum GT Lode dependent model cell. Figs. 7 (a) and (c) represent the evolution of the macroscopic effective stress Σ_e normalized by the initial yield stress, σ_0, as a function of the macroscopic effective strain E_e, and Figs. 7 (b) and (d) exhibit the porosity evolution f with E_e. The results of the simulations are plotted until reaching the coalescence deformation E_c.

The fitting parameters k_Ω for the modified GT model simulations are k_Ω= 0.0, (which retrieves the classical GT model), 0.01, 0.03 and 0.04. The q_1 and q_2 parameters are the interpolated values obtained from Eq.(22) for $T = 1$.

Quantitative differences in the prediction of material ductile behaviour are observed for the modified GT model when different k_Ω values are used in the simulations. For $k_\Omega = 0.0$ the modified GT model behaves underestimating the stress-strain curve of the voided J_2 cell and overpredicting the void volume fraction evolution. The opposite tendency (overpredicting stress strain behaviour and underestimating porosity growth rate) is observed when k_Ω is equal to 0.04. Then, with a proper choice of the k_Ω parameter, it is possible to match the stress-strain and void growth rate curves of a GT-Lode dependent material to those predicted by the voided cell analysis. In this case $k_\Omega = 0.03$ is the value that better fits the behaviour of the material.

Figs. 8 present analogous results for $f_0 = 0.005$ and $f_0 = 0.01$ prescribing in this case $T = 1$ and $L = 1$. The curves show that the proposed model, with a proper selection of k_Ω ($k_\Omega = 0.03$) agrees very well with that obtained from the voided cell analysis for both void volume fraction and stress-strain response.

Similarly, in Figs.(9) and (10), where $T = 2$, $L = 0$ (Figs.9 (a)-(d)) and $L = 1$ (Figs. 10 (a)-(d)), the k_Ω parameter that more accurately predict the stress-strain relations and void volume fraction evolution of the J_2 voided cell is $k_\Omega = 0.03$ for $L = 0$ and a k_Ω value within the range $(0.01, 0.03)$ for $L = 1$ for both initial porosities $f_0 = 0.005$ and $f_0 = 0.01$.

The cases with triaxility $T = 1.5$ and $L = 0$ and $L = 1$ lead to similar results.

A final remark is that the proposed new approach and the calibrated (q_{1mod}, q_{2mod}) val-

ues improve the Gurson model but it is still imperfect. It is obvious that further numerical studies and comparisons with experimental results are necessary to further verify/calibrate the proposed modification of the Gurson model.

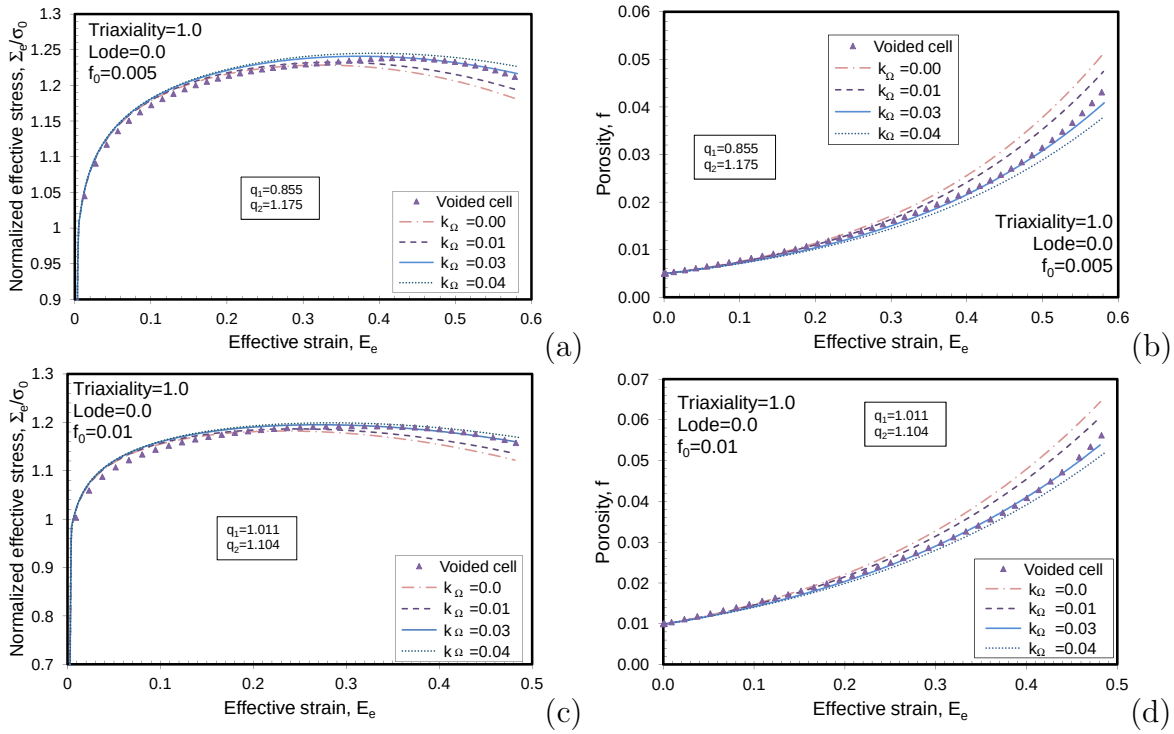

Figure 7: Σ_e versus E_e and f versus E_e for $f_0 = 0.005$ (a, b) and $f_0 = 0.01$ (c, d). $T = 1$, $L = 0$.

7. Concluding remarks

The salient feature of the present paper is the proposition of an improved GT model that accounts for the triaxiality and Lode effects through q_1 and q_2. We also present the finite element implementation of the modified GT model using return mapping method (Euler-backward integration technique) and the formulation of the consistent tangent modulus. An extension of the computational cell model employed by Xia and Shih (1995 a,b, 1996) has been developed to prescribe both macroscopic triaxiality and Lode parameter, and several numerical simulations are presented for Weldox 960 steel with different initial porosities and for distinct prescribed T and L values. The q_1 and q_2 classical GT parameters have been calibrated for $L = -1$ and extended to other possible Lode parameters values. The convexity of the proposed yield modified Gurson locus is assured. The obtained results

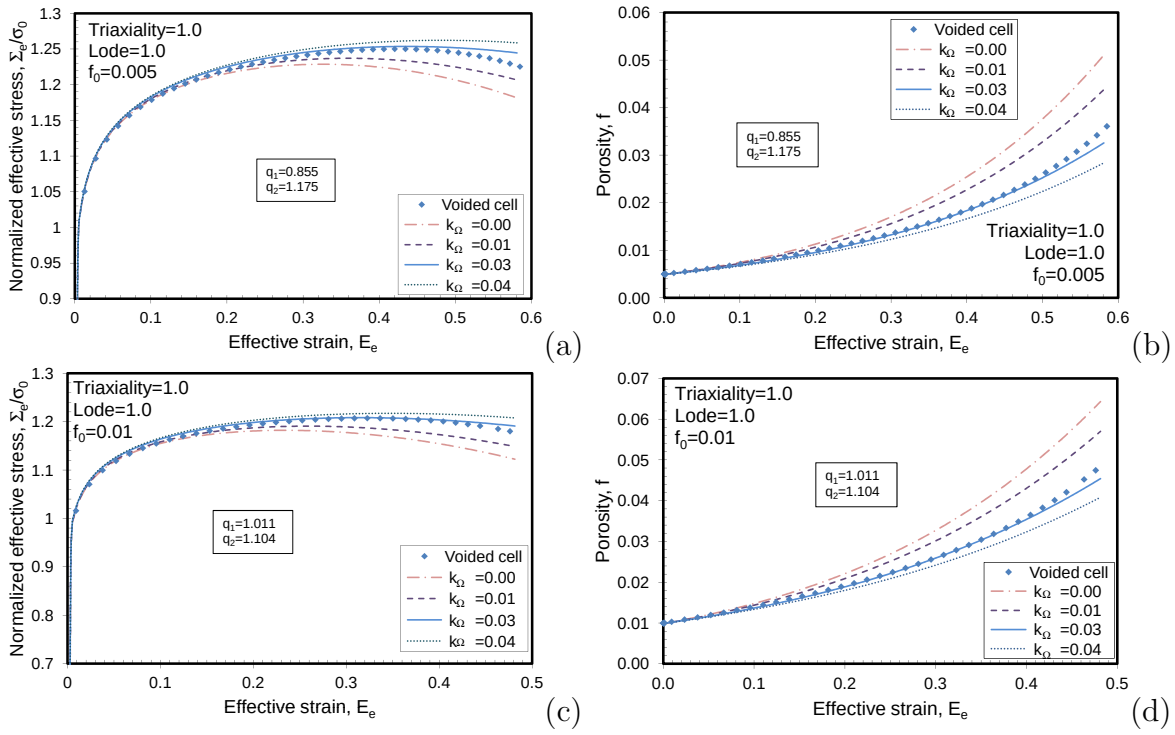

Figure 8: Σ_e versus E_e and f versus E_e for $f_0 = 0.005$ (a, b) and $f_0 = 0.01$ (c, d). $T = 1$, $L = 1$.

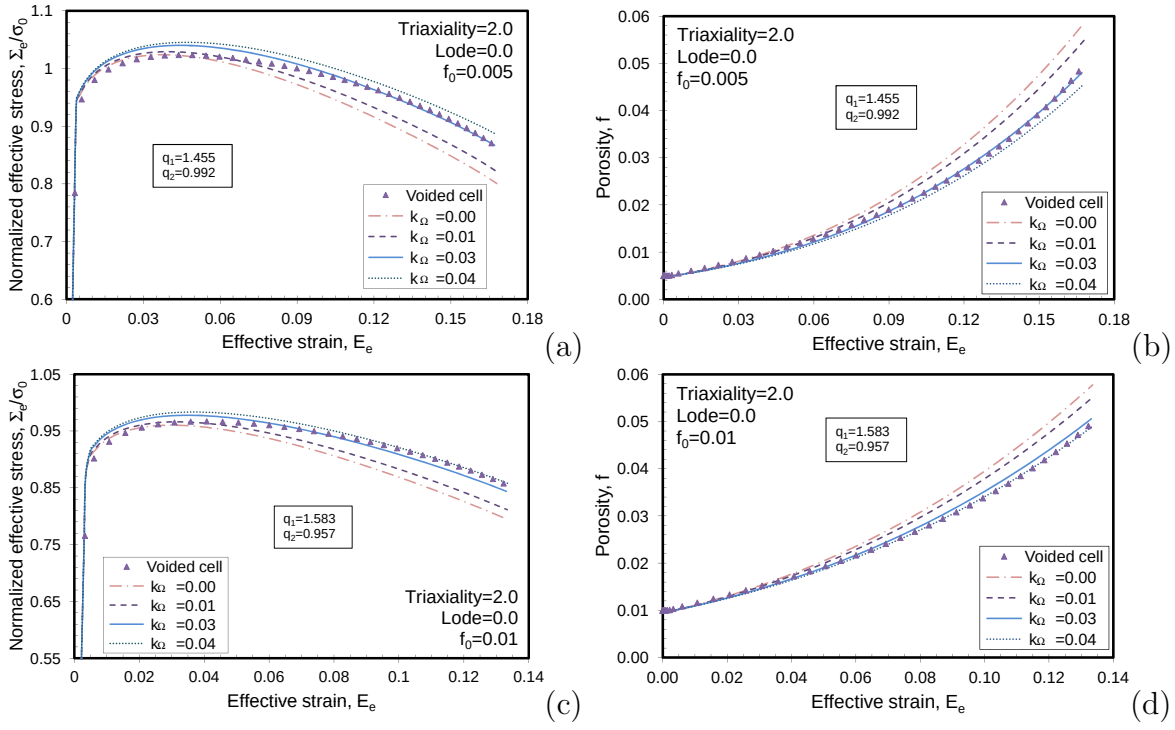

Figure 9: Σ_e versus E_e and f versus E_e for $f_0 = 0.005$ (a, b) and $f_0 = 0.01$ (c, d). $T = 2$, $L = 0$.

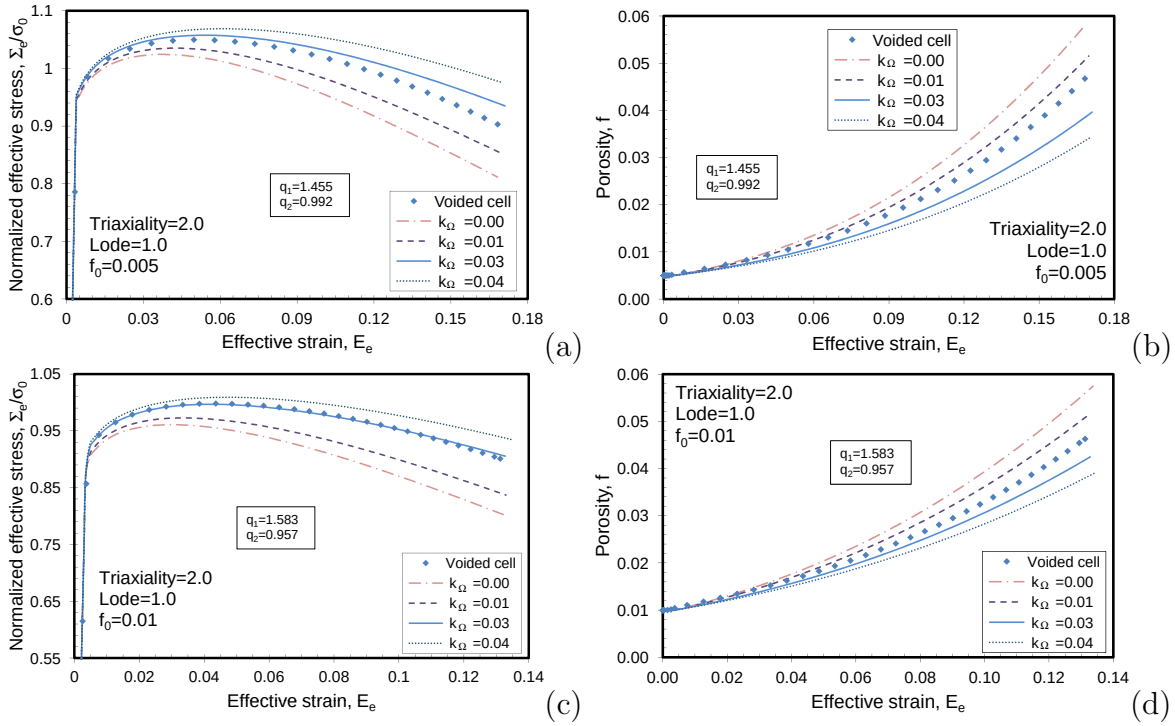

Figure 10: Σ_e versus E_e and f versus E_e for $f_0 = 0.005$ (a, b) and $f_0 = 0.01$ (c, d). $T = 2$, $L = 1$.

show good agreement between the two cell models (the voided J_2 and the proposed continuum damage model cells) for the triaxialities and Lode parameters tested (T =1, 1.5, 2 and $L = 0,\ 1$).

At high triaxialities, the proposed modified GT model permits to extend predictions to any Lode parameter and expands its applicability in order to have better agreement with the J_2 finite element analyses with a unitary voided cell.

Acknowledgements

The authors are indebted to the Ministerio de Economía y Competitividad (Projects DPI2011-23191 and DPI/2011-24068) for the financial support received which allowed conducting part of this work.

The authors would like to thank Professor J. Faleskog, Royal Institute of Technology (KTH) of Sweden, and Dr. J.A. Rodríguez-Martínez and Dr. J. Zahr, University Carlos III of Madrid (UC3M), for valuable discussions.

Appendix A.

- Operating $\mathbf{\Sigma}'^{trial} : \mathbf{\Sigma}'^{trial}$ from Eq. (38) considering the identities given in Eq.(37) and Eqs.(43), it follows:

$$\left(\Sigma_e^{trial}\right)^2 = \left(\Sigma_e + 3G\Delta\varepsilon_q\right)^2 + \left(2G\Delta\varepsilon_\Omega\right)^2 \left(\frac{27}{2\Sigma_e^2} - \frac{3\cdot 81^2}{8}\frac{J_3^2}{\Sigma_e^8}\right)\cdot\frac{3}{2} \tag{A.1}$$

- Taking into account the relation $\mathbf{\Sigma}' : \mathrm{cof}\left(\mathbf{\Sigma}'\right) = 3J_3$, Eqs (40) and (42) allows J_3^{trial} to be written as function of the stress measures J_3 and Σ_e as:

$$J_3^{trial} = J_3\, X^3 + Y^3\, \left(J_3^2 - \frac{2}{729}\,\Sigma_e^6\right) + \frac{2}{27}X^2\, Y\;\; \Sigma_e^4 + \frac{J_3\,\Sigma_e^2\, X\, Y^2}{3} \tag{A.2}$$

being X, Y, Z and J_3:

$$X = 1 + \frac{3G}{\Sigma_e}\Delta\varepsilon_q - \frac{243\; G\; J_3}{2\Sigma_e^5}\Delta\varepsilon_\Omega;\;\; Y = \frac{27G}{\Sigma_e^3}\Delta\varepsilon_\Omega;\; Z = \frac{\Sigma_e^2\, Y}{9};\; J_3 = \frac{2\Sigma_e^3}{27}(\Omega+1)$$

Appendix B.

- Deriving Eqs. (48a-b), $\partial\Sigma_h$ and $\partial\Sigma_e$ have the form.

$$\begin{aligned} &\partial\Sigma_h = \partial\Sigma_h^{trial} - K\partial\Delta\varepsilon_p; \\ &\partial\Sigma_e = A_{11}\partial\Sigma_e^{trial} + A_{12}\partial\Delta\varepsilon_q + A_{13}\partial\Delta\varepsilon_\Omega + A_{14}\partial\Omega; \qquad A_{ij}\text{ coefficients known} \end{aligned} \tag{B.1}$$

and the values $\partial\Delta\varepsilon_p$, $\partial\Delta\varepsilon_q$ and $\partial\Delta\varepsilon_\Omega$ obtained from the five implicit constitutive equations given in Eqs.(47) and the relations obtained in Eqs.(B.1):

$$\begin{aligned} \partial\Delta\varepsilon_p &= B_{11}\partial\Sigma_h^{trial} + B_{12}\partial\Sigma_e^{trial} + B_{13}\partial\Omega \\ \partial\Delta\varepsilon_q &= B_{21}\partial\Sigma_h^{trial} + B_{22}\partial\Sigma_e^{trial} + B_{23}\partial\Omega \\ \partial\Delta\varepsilon_\Omega &= B_{31}\partial\Sigma_h^{trial} + B_{32}\partial\Sigma_e^{trial} + B_{33}\partial\Omega; \qquad B_{ij}\text{ coefficients known} \end{aligned} \tag{B.2}$$

- From the derivation of Eq. (48.c):

$$\begin{aligned} &3\left(\Omega+1\right)X^2\partial X + X^3\partial\Omega + \left(2\left(\Omega+1\right)^2 - 1\right)\frac{\left(Y\Sigma_e\right)^2}{9}\partial(Y\Sigma_e) + 4\frac{\left(Y\Sigma_e\right)^3}{27}\left(\Omega+1\right)\partial\Omega + \\ &+2X\left(Y\Sigma_e\right) + X^2\partial(Y\Sigma_e) + \frac{\left(Y\Sigma_e\right)^2}{3}\left(\Omega+1\right)\partial X + \frac{2X\left(\Omega+1\right)}{3}\left(Y\Sigma_e\right)\partial\left(Y\Sigma_e\right) + \\ &+\frac{X\left(Y\Sigma_e\right)^2}{3}\partial\Omega = \frac{27}{2\Sigma_e^3}\partial J_3^{trial} - \frac{81J_3^{trial}}{2\Sigma_e^4}\partial\Sigma_e \end{aligned} \tag{B.3}$$

being ∂X and $\partial\left(Y\Sigma_e\right)$ the derivades of X and $(Y\Sigma_e)$ from Eqs. (45):

$$\partial X = 3G\frac{\partial\Delta\varepsilon_q}{\Sigma_e} - \frac{9G\left(\Omega+1\right)}{\Sigma_e^2}\partial\Delta\varepsilon_\Omega - \frac{9G\Delta\varepsilon_\Omega}{\Sigma_e^2}\partial\Omega + \left(\frac{18G\left(\Omega+1\right)\Delta\varepsilon_\Omega}{\Sigma_e^3} - 3G\frac{\Delta\varepsilon_q}{\Sigma_e^2}\right)\partial\Sigma_e$$
$$\partial\left(Y\Sigma_e\right) = \frac{-54G\Delta\varepsilon_\Omega}{\Sigma_e^3}\partial\Sigma_e + \frac{27G}{\Sigma_e^2}\partial\Delta\varepsilon_\Omega \tag{B.4}$$

$\partial\Omega$ can be written after operating in Eqs. (B.3, B.1b, B.4) as:

$$\partial\Omega = B_{41}\partial\Delta\varepsilon_q + B_{42}\partial\Delta\varepsilon_\Omega + B_{43}\partial\Sigma_e^{trial} + B_{44}\partial J_3^{trial} \tag{B.5}$$

or in a similar manner, considering the relation given in Eqs. (B.2b, B.2c):

$$\partial\Omega \;=\; \tilde{B}_{41}\partial\Sigma_h^{trial} + \tilde{B}_{42}\partial\Sigma_e^{trial} + \tilde{B}_{43}\partial J_3^{trial} \tag{B.6}$$

that allows $\partial\Delta\varepsilon_p$, $\partial\Delta\varepsilon_q$ and $\partial\Delta\varepsilon_\Omega$ to be written as:

$$\begin{aligned}
\partial\Delta\varepsilon_p &= \tilde{B}_{11}\partial\Sigma_h^{trial} + \tilde{B}_{12}\partial\Sigma_e^{trial} + \tilde{B}_{13}\partial J_3^{trial} \qquad (B.7)\\
\partial\Delta\varepsilon_q &= \tilde{B}_{21}\partial\Sigma_h^{trial} + \tilde{B}_{22}\partial\Sigma_e^{trial} + \tilde{B}_{23}\partial J_3^{trial}\\
\partial\Delta\varepsilon_\Omega &= \tilde{B}_{31}\partial\Sigma_h^{trial} + \tilde{B}_{32}\partial\Sigma_e^{trial} + \tilde{B}_{33}\partial J_3^{trial} \qquad \tilde{B}_{ij} \text{ values known}
\end{aligned}$$

- Deriving the relation given in Eq. (42):

$$(2X\partial X - Y\partial Z - Z\partial Y)\mathrm{cof}\left(\boldsymbol{\Sigma}'\right) + (X^2 - YZ)\boldsymbol{\partial}\left(\mathrm{cof}\boldsymbol{\Sigma}'\right) = \tag{B.8}$$
$$\boldsymbol{\partial}\left(\mathrm{cof}\boldsymbol{\Sigma}'^{trial}\right) - \left(2Z\partial X + 2X\partial Z + 2YJ_3\partial Y + Y^2\partial J_3\right)\boldsymbol{\Sigma}' - \left(2XZ + Y^2J_3\right)\boldsymbol{\partial\Sigma}' +$$
$$+ \left(YJ_3\partial X + XJ_3\partial Y + XY\partial J_3 + 4Z\partial Z\right)\mathbf{1}$$

with ∂X given in Eq. (B.4a), and ∂Y and ∂Z obtained from Eqs. (A.3) and with the form:

$$\partial Y = \frac{27G}{\Sigma_e^3}\partial\Delta\varepsilon_\Omega - \frac{81G}{\Sigma_e^4}\partial\Sigma_e; \quad \partial Z = \frac{\Sigma_e^2}{9}\partial Y + \frac{2Y\Sigma_e}{9}\partial\Sigma_e \tag{B.9}$$

and ∂J_3 as:

$$\partial J_3 = \frac{6\Sigma_e^2\left(\Omega+1\right)}{27}\partial\Sigma_e + \frac{2\Sigma_e^3}{27}\partial\Omega \tag{B.10}$$

it is possible to obtain, considering Eqs. (B.1a, B.4a, B.6, B.7, B.8, B.9, B.10):

$$\boldsymbol{\partial}\left(\mathrm{cof}\boldsymbol{\Sigma}'\right) = \tilde{C}_1\boldsymbol{\partial}\left(\mathrm{cof}\boldsymbol{\Sigma}'^{trial}\right) + \tilde{C}_2\boldsymbol{\partial\Sigma}' + \tilde{D}_1\boldsymbol{\Sigma}' + \tilde{D}_2\mathrm{cof}\left(\boldsymbol{\Sigma}'\right) + \tilde{D}_3\mathbf{1} \tag{B.11}$$

being $\tilde{D}_1$, $\tilde{D}_2$ and $\tilde{D}_3$ of the form: $\tilde{D}_i = \tilde{D}_{i1}\partial\Sigma_h^{trial} + \tilde{D}_{i2}\partial\Sigma_e^{trial} + \tilde{D}_{i3}\partial J_3^{trial}$
with $\tilde{C}_1$, $\tilde{C}_2$ and all $\tilde{D}_{ij}$ coefficients known.

References

Aravas, N., 1987. On the numerical integration of a class of pressure-dependent plasticity models. International Journal of Numerical Methods in Engineering 24, 1395–1416.

Bai, Y., Wierzbicki, T., 2008. A new model of metal plasticity and fracture with pressure and lode dependence. International Journal of Plasticity 24, 1071–1096.

Bao, Y., Wierzbicki, T., 2004. On fracture locus in the equivalent strain and stress triaxiality space. International Journal of Mechanical Sciences 46, 81–98.

Barsoum, I., Faleskog, J., 2007. Rupture mechanisms in combined tension and shear: Micromechanics. International Journal of Solids and Structures 44, 5481–5498.

Barsoum, I., Faleskog, J., 2011. Micromechanical analysis on the influence of the Lode parameter on void growth and coalescence. International Journal of Solids and Structures 48, 925–938.

Barsoum, I., Faleskog, J., Pingle, S., 2011. The influence of the Lode parameter on ductile failure strain in steel. Procedia Engineering 10, 69–75.

Benallal, A., Desmorat, R., Fournage, M., 2014. An assessment of the role of the third stress invariant in the gurson approach for ductile fracture. European Journal of Mechanics A/Solids 47, 400–414.

Benzerga, A., 2002. Micromechanics of coalescence in ductile fracture. Journal of the Mechanics and Physics of Solids 50, 1331–1362.

Besson, J., 2010. Continuum models of ductile fracture: A review. International Journal of Damage Mechanics 19, 3–52.

Brünig, M., Chyra, O., Albrecht, D., Driemeier, L., Alves, M., 2008. A ductile damage criterion at various stress triaxialities. International Journal of Plasticity 24, 1731–1755.

Danas, K., Ponte-Castañeda, P., 2012. Influence of the Lode parameter and the stress triaxiality on the failure of elasto-plastic porous materials. International Journal of Solids and Structures 49, 1325–1342.

Faleskog, J., Gao, X., Shih, C., 1998. Cell model for nonlinear fracture analysis I. micromechanics calibration. International Journal of Fracture 89(4), 355–373.

Flandi, L., Leblond, J. B., 2005 b. A new model for porous viscoplastic solids incorporating void shape effects II: Numerical validation. European Journal of Mechanics 24, 552–571.

Gao, X., Faleskog, J., Shih, C. F., 1998. Ductile tearing in part-throgh cracks: Experiments and cell-model predictions. Engineering Fracture Mechanics 59, 761–777.

Gao, X., Kim, J., 2006. Modeling of ductile fracture: Significance of void coalescence. International Journal of Solids and Structures 43, 6277–6293.

Gao, X., Whang, T., Kim, J., 2005. On ductile fracture initiation toughness: Effects of void volume fraction, void shape and void distribution. International Journal of Solids and Structures 42, 5097–5117.

Gao, X., Zhang, T., Hayden, M., Roe, C., 2009. Effects of the stress state on plasticity and ductile failure of an aluminum 5083 alloy. International Journal of Plasticity 25, 2366–2382.

Gao, X., Zhang, T., Zhou, J., Graham, S. M., Hayden, M., Roe, C., 2011. On stress-state dependent plasticity modeling: Significance of the hydrostatic stress, the third invariant of stress deviator and the non-associated flow rule. International Journal of Plasticity 27, 217–231.

Gologanu, M., Leblond, J., Perrin, G., Devaux, J., 1997. Recent extensions of Gursons model for porous ductile metals. P. Suquet (Ed.), Continuum Micromechanics, Springer Verlag.

Gărăjeu, M., Michel, J.-C., Suquet, P., 2000. A micromechanical approach of damage in viscoplastic materials by evolution in size shape and distribution of voids. Computational Methods in Applied Mechanical Engineering 183, 223–246.

Gurson, A. L., 1977. Continuum theory of ductile rupture by void nucleation and growth part I. yield criteria and flow rules for porous ductile media. Journal of Engineering Materials and Technology 99, 2–15.

Hill, R., 1967. The essential structure of constitutive laws for metal composites and polycrystals. Journal of the Mechanics and Physics of Solids 15, 79–95.

Jackiewicz, J., 2011. Use of a modified Gurson model approach for the simulation of ductile fracture by growth and coalescence of microvoids under low, medium and high stress triaxiality loadings. Engineering Fracture Mechanics 78, 487–502.

Kim, J., Gao, X., Srivatsan, T. S., 2003. Modeling of crack growth in ductile solids: a three-dimensional analysis. International Journal of Solids and Structures 40, 7357–7374.

Kim, J., Gao, X., Srivatsan, T. S., 2004. Modeling of void growth in ductile solids: effects of stress triaxiality and initial porosity. Engineering Fracture Mechanics 71, 379–400.

Kim, J., Zhang, G., Gao, X., 2007. Modeling of ductile fracture: Application of the mechanism-based concepts. International Journal of Solids and Structures 44, 1844–1862.

Koplik, J., Needleman, A., 1988. Void growth and coalescence in porous plastic solids. International Journal of Solids and Structures 24, 835–53.

McClintock, F. A., 1968. A criterion for ductile fracture by the growth of holes. Journal of Applied Mechanics 35, 363–371.

Monchiet, V., Cazacu, O., Charkaluk, E., Kondo, D., 2008. Macroscopic yield criteria for plastic anisotropic materials containing spheroidal voids. International Journal of Plasticity 24, 1158–1189.

Nahshon, K., Hutchinson, J. W., 2008. Modification of the Gurson Model for shear failure. European Journal of Mechanics - A/Solids 27, 1–17.

Pardoen, T., Hutchinson, J. W., 2000. An extended model for void growth and coalescence. International Journal of the Mechanics and Physics of Solids 48, 2467–2512.

Pietryga, M., Vladimirov, I., Reese, S., 2012. A finite deformation model for evolving flow anisotropy with distortional hardening including experimental validation. Mechanics of Materials 44, 163–173.

Pineau, A., Pardoen, T., 2007. Comprehensive structural integrity encyclopedia. vol. 2. Amsterdam: Elsevier [chapter 6].

Rice, J. R., Tracey, D. M., 1969. On the ductile enlargement of voids in triaxial stress fields. Journal of the Mechanics and Physics of Solids 17, 201–217.

Simo, J., Taylor, R. L., 1985. Consistent tangent operators for rate-independent elastoplasticity. Computer Methods in Applied Mechanics and Engineering 48, 101–118.

Simulia, 2014. ABAQUS/Standard User's Manual, version 6.14 Edition. Dassault Systèmes, Providence, USA.

Tvergaard, V., 1981. Influence of voids on shear band instabilities under plane strain conditions. International Journal of Fracture 17, 389–407.

Tvergaard, V., 1982. On localization in ductile materials containing spherical voids. International Journal of Fracture 18, 237–252.

Vadillo, G., Fernández-Sáez, J., 2009. An analysis of Gurson model with parameters dependent on triaxiality based on unitary cells. European Journal of Mechanics A/Solids 28, 417–427.

Wen, J., Huang, Y., Hwang, K. C., Liu, C., Li, M., 2005. The modified Gurson model accounting for the void size effect. International Journal of Plasticity 21, 381–395.

Xia, L., Shih, C. F., 1995 a. Ductile crack growth- I. A numerical study using computational cells with microstructurally based length scales. Journal of the Mechanics and Physics of Solids 43, 233–259.

Xia, L., Shih, C. F., 1995 b. Ductile crack growth- II. Void nucleation and geometry effects on macroscopicvfracture behavior. Journal of the Mechanics and Physics of Solids 43, 1953–1981.

Xia, L., Shih, C. F., 1996. Ductile crack growth - III. Transition to cleavage fracture incorporating statistics. Journal of the Mechanics and Physics of Solids 44, 603–639.

Xue, L., 2007. Damage accumulation and fracture initiation in uncracked ductile solids subject to triaxial loading. International Journal of Solids and Structures 44, 5163–5181.

Xue, L., 2008. Constitutive modeling of void shearing effect in ductile fracture of porous materials. Engineering Fracture Mechanics 75, 3343–3366.

Yamamoto, H., 1978. Conditions for shear localization in the ductile fracture of void containing materials. International Journal of Fracture 14, 347–365.

Zhang, K. S., Bai, J. B., François, D., 2001. Numerical analysis of the influence of the Lode parameter on void growth. International Journal of Solids and Structures 38, 5847–5856.

Zhang, Z. L., 1995. On the accuracies of numerical integration algorithms for Gurson-based pressure-dependent elastoplastic constitutive models. Computer Methods in Applied Mechanics and Engineering 121, 15–28.

Zhang, Z. L., Thaulow, C., Ødegård, J., 2000. A complete Gurson model approach for ductile fracture. Engineering Fracture Mechanics 67, 155–168.